Vacuum-annealing induces sub-surface redox-states in surfactant-structured α-Fe$_2$O$_3$ photoanodes prepared by ink-jet printing

Alexander N. Bondarchuk[a,*], Laurence M. Peter[b], Gabriela P. Kissling[b], Elena Madrid[b], Josué A. Aguilar-Martínez[c], Zuhayr Rymansaib[d], Pejman Iravani[d], Murilo Gromboni[e], Lucia H. Mascaro[e], Aron Walsh[b], Frank Marken[b,*]

[a] Technological University of Mixteca, Huajuapan 69000, Oaxaca, Mexico
[b] Department of Chemistry, University of Bath, Bath BA2 7AY, UK
[c] Universidad Autónoma de Nuevo León, Facultad de Ingeniería Mecánica y Eléctrica, Centro de Investigación e Innovación en Ingeniería Aeronáutica (CIIIA), Carretera a Salinas Victoria km 2.3, C.P. 66600, Apodaca, N.L., Mexico
[d] Department of Mechanical Engineering, University of Bath, Bath BA2 7AY, UK
[e] Department of Chemistry, San Carlos Federal University, Rod. Washigton Luiz, km 235, CEP 13565-905, São Carlos, SP, Brazil

ARTICLE INFO

ABSTRACT

Transparent nano-structured hematite (α-Fe$_2$O$_3$) films of approximately 550 nm thickness on tin-doped indium oxide (ITO) have been obtained conveniently by ink-jet printing of a Fe(NO$_3$)$_3$/Brij® O10 precursor ink and subsequent annealing at 500 °C in air. When illuminated with a blue LED (λ = 455 nm, ca. 100 mW cm^{-2}), the hematite films exhibited photocurrents of up to 70 μA cm^{-2} at 0.4 V vs. SCE in 0.1 M NaOH electrolyte. Thermal annealing in vacuum at 500 °C for 2 h increased photocurrents more than three times to 230 μA cm^{-2} in agreement with previous literature reports for pure hematite materials. These results suggest that a simple ink-jetting process with surfactants is viable. The effects of vacuum-annealing on the photoelectrical properties of α-Fe$_2$O$_3$ films are discussed in terms of a sub-surface state templating hypothesis based on data gathered from photo-transients, field emission scanning electron microscopy, X-ray photoelectron spectroscopy analysis, X-ray diffraction, photocurrent spectra, and cyclic voltammetry.

© 2017 Elsevier B.V. All rights reserved.

1. Introduction

One of the greatest challenges of our century is the search for new energy sources, which are economical and safe, possibly distributed, and which avoid pollution of the environment. The development of solar technologies can provide clean and renewable energy when based on an energy vector such as hydrogen. Therefore, the direct solar production of hydrogen and oxygen through solar water splitting [1] could be a promising technology. The method can be based on photo-electrolysis of water into O$_2$ (at the photoanode) and H$_2$ (at the photocathode) on the surface of suitable photo-active materials under solar illumination [2,3]. Pursuing this approach requires development of appropriate photo-electrode materials, which must fulfill requirements such as strong/effective light absorption, suitable band edge position for reduction/oxidation of water and high chemical stability [4,5]. In addition, such material should be based on low cost components and be suitable for low cost fabrication of electrodes also on large area. A particularly attractive fabrication tool today is printing and therefore ink-jet printing has been employed in this study based on a Fe(NO$_3$)$_3$/Brij® O10 surfactant ink to produce nano-structured films of hematite.

A promising candidate for photo-anode applications is α-Fe$_2$O$_3$ (hematite [6–8]), which has a suitable band gap (~2 eV) ideal for visible light harvesting [9–11], low cost, earth abundance, is non-toxic, and possesses good stability in aqueous media. In theory, this semiconducting material can produce a photocurrent density of ca. 4 mA cm^{-2} (for single pass flat interfaces) or up to ca. 12 mA cm^{-2} (for nano-structured interfaces [12]) under AM 1.5 solar spectral illumination. However, with varying film fabrication methodologies performance can change. Also, with pure hematite

* Corresponding authors.
E-mail addresses: alexbondua@yahoo.com (A.N. Bondarchuk), f.marken@bath.ac.uk (F. Marken).

(without catalyst layers) such photocurrent has not been achieved in practice because of (i) fast recombination of photo-generated charge carriers in the bulk and at surface states in α-Fe$_2$O$_3$ [13], (ii) slow surface kinetics associated with the formation of oxygen [14], and (iii) poor electrical conductivity within the un-doped material ($\sim$10^{-2} cm^2 V^{-1} s^{-1} [15]), but also inter-grain conductivity related problems to a very short hole diffusion length, around 2–4 nm [16] or in some materials reported even shorter (0.5–1.5 nm [17]). The electrical conductivity in α-Fe$_2$O$_3$ is anisotropic because of its hexagonal crystal structure with antiferromagnetic magnetic structure [18–20]. Hematite exhibits a typical optical thickness of 45 nm at a wavelength of 400 nm [21], which means that only thin layers of material are active. Therefore, based on pure hematite it is difficult to develop photoanodes with a photocurrent approaching the theoretical limit. Nevertheless, new approaches to the formation of thin hematite films can be useful and a comparison of properties based on pure hematite films is needed.

To improve the photo-electrochemical properties of α-Fe$_2$O$_3$ structures, different strategies are applied including doping of hematite to increase conductivity [22,23], coupling hematite with other oxides in heterojunctions to enhance a charge carrier collection [24], application of nano-textured conductive substrates for more efficient charge collection [25,26], surface/interface passivation layers for reduced surface/interface charge recombination [27–29], and catalyst adsorption for accelerated interfacial water oxidation kinetics [30–32]. Recently, it has been reported that the incorporation of oxygen vacancies into hematite photoelectrodes can be an effective approach to improve photocurrents and activity for water oxidation [33,34]. To produce oxygen vacancies in α-Fe$_2$O$_3$, both plasma treatment and high-temperature treatment of films under an atmosphere of H$_2$ or Ar can be employed [35]. Instead of an argon atmosphere annealing also vacuum annealing may be used as has been demonstrated by Joo et al. [36] and by Ling et al. [37] and is employed in this report. Considerable effects of oxygen vacancy doping on conductivity have been noted similar to those observed by stannate doping. In addition to conductivity changes induced by oxygen vacancies, it is interesting to note possible links in chemistry (i) when oxygen is extracted from hematite at elevated temperatures and (ii) during ambient oxygen evolution in contact to aqueous electrolyte.

Photoelectrochemical processes within the photo-excited hematite film are complex in particular in non-planar nano-structured films, but can be simplified based on some predominant phenomena, which are shown schematically in Fig. 1 for photo-transient current responses for "light-on" and "light-off" transients.

When switching on the illumination, an anodic current spike shows that charge carrier separation occurs with holes being captured at surfaces and electrons diffusing into the substrate electrode (see Fig. 1B). When switching off the illumination the remaining holes may cause a flow of electron back into the hematite film (see Fig. 1C) resulting into a cathodic current spike.
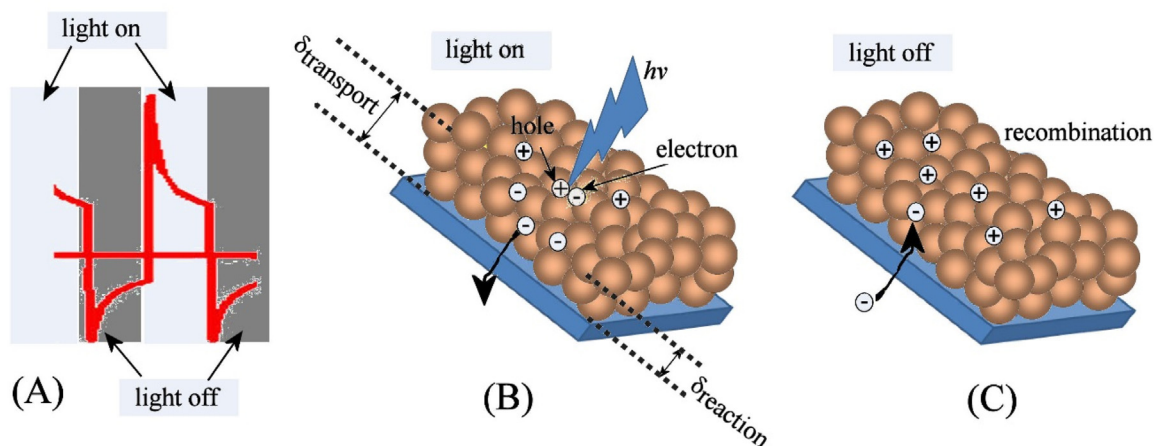
Net anodic current has to be attributed to the formation of oxygen from water and the rate for this process can be represented by a first order rate constant k_{tr}. This process is competing with recombination represented here by the first order rate constant k_{rec}. The fraction of holes that successfully transfer to generate oxygen is given by $\eta_{trans} = k_{tr}/(k_{tr} + k_{rec})$ [38], which is a measure of the resulting anodic steady state photocurrent. The transient decay is governed by $k_{tr} + k_{rec}$ [39] and the approximate decay time of $\tau = \frac{1}{k_{tr}+k_{rec}}$. Both of these two rate constants may be affected by electron charge mobility in the semiconductor. A corresponding reaction layer may be expressed as $\delta_{reaction} = \sqrt{\frac{D_{electron}}{k_{tr}+k_{rec}}}$ (with $D_{electron}$ indicating the apparent diffusion coefficient for electrons). "Harvesting" of electrons from the film into the substrate electrode may also be indicated as an apparent transport layer, $\delta_{transport}$, which is dependent on electron mobility as well as the applied bias voltage (see Fig. 1B). Both $\delta_{reaction}$ or $\delta_{transport}$ can be associated with the rate/photo-current limiting process.

In this work we report formation of nano-structured α-Fe$_2$O$_3$ films prepared by ink-jet printing and the enhancement of photo-electrochemical properties after thermal annealing in vacuum at 500 °C. Effects are discussed based on the data from photoelectrochemical transients, field emission scanning electron microscopy (FE-SEM), X-ray diffraction, X-ray photoelectron spectroscopy (XPS) analysis, photocurrent spectra, and cyclic voltammetry. We suggest that printed films provide a promising research tool as well as being economical for devices. In the future, ink-jet printing could provide a reproducible and cost-effective way to: (i) develop photo-electrodes with larger area, (ii) introduce dopants and composite components, (iii) study effects of gradual (sub-surface state) doping during vacuum-annealing, and (iv) control nano-structure morphology and thickness.
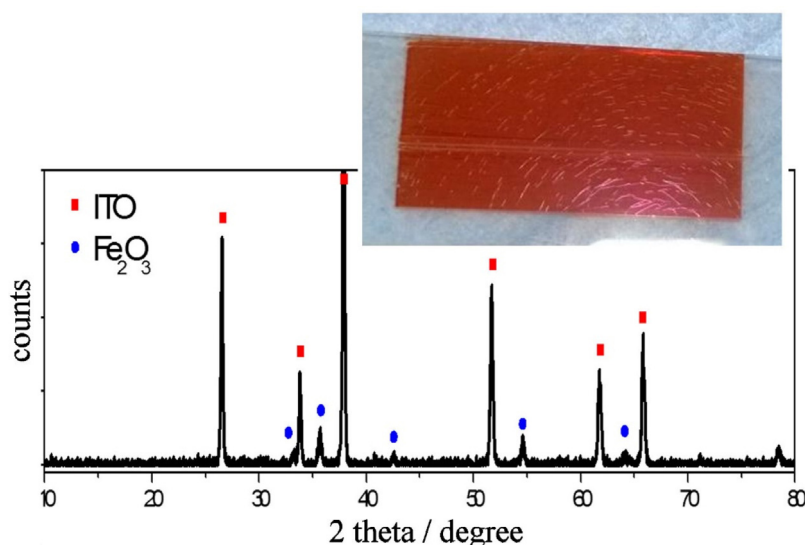
2. Experimental

2.1. Preparation and annealing of α-Fe$_2$O$_3$ films

Thin films of α-Fe$_2$O$_3$ were prepared by ink-jet printing (on a Fujifilm DMP-2800 printer with substrates heated to 60 °C) of a

Fig. 1. Schematic drawing of (A) light-on and light-off photocurrent transients, (B) the flow of electrons from hematite into the substrate upon switching on the illumination, and (C) the flow of electrons back into the hematite upon switching off the illumination.

Fig. 2. X-ray diffraction patterns for the film deposited on ITO substrate (blue circle α-Fe$_2$O$_3$ (hematite) and red rectangle tin-doped indium oxide or ITO). Also shown is a photograph of the orange coloured transparent hematite film on glass. (For interpretation of the references to colour in this figure legend, the reader is referred to the web version of this article.)

hematite precursor ink onto glass substrates coated by tin-doped indium oxide (ITO, obtained from Image Optics Components, Basildon, UK) and subsequently annealing at 500 °C for 2 h in air with a heating/cooling rate of 3 °C/min in a tube furnace (Elite Thermal Systems Ltd., UK). The precursor solution was obtained by dissolving 0.5 g of Fe(NO$_3$)$_3$· 9 H$_2$O (99.95%, Sigma-Aldrich) in 1 mL of ethanol with 0.2 mL of surfactant Brij® O10 (Sigma-Aldrich). The solution was filtered with a 1.2 μm pore syringe filter before printing. ITO substrates were cleaned by sequential sonication in acetone (30 min) and in ethanol (30 min), washing in deionized water, drying and heating to 500 °C for 1 h in air. Annealing of α-Fe$_2$O$_3$ films in vacuum (Speedivac Edwards High Vacuum Pump ED50, Crawley, England) was performed at 500 °C for 2 h in a quartz tube, which was placed into the tube furnace. The vacuum in the tube was maintained during heating and cooling.

2.2. Structural and morphological characterization

The morphology and thickness of the films were evaluated by high-resolution field emission scanning electron microscopy (FE-SEM, Zeiss Supra 35 at 2 kV). X-ray diffraction (XRD) patterns were recorded using a PANalytical Empyrean diffractometer with CuKα radiation (λ = 1.5406 Å) operated at 45 kV and 40 mA. Scans were done in the 2&z.Theta; range from 10° to 80° in steps of 0.02° and 1 s per step in a continuous mode using grazing incidence technique with an incidence angle of 1°. The crystalline phases were identified using X'Pert High Score Plus software and ICSD database (ICSD – Inorganic Crystal Structure Database). X-ray photoelectron spectroscopy (XPS) spectra were recorded with a Thermo Scientific Inc., Model K-Alpha Surface Analysis. Monochromatic Al Kα radiation (E = 1486.68 eV) was used.

2.3. Electrochemical testing

Electrochemical measurements were performed with an Autolab potentiostat/galvanostat instrument PGSTAT30 (Ecochemie, Netherlands) with Autolab GPES software. Photocurrents were recorded with back illumination by using a three-electrode configuration with a Pt-wire counter electrode, a working electrode with area of 1 cm^2, and a KCl-saturated calomel (SCE) reference electrode. Electrolyte solutions were 0.1 M NaOH in deminer-

alised water. The light was generated by the blue light-emitting diode M455L2 (455 nm, Thorlabs M455L2) which was controlled by LED driver (T-Cube LED driver, Thorlabs, UK) and a DDS Function/Arbitrary TG4001 Generator (TTi, UK). The light chopping frequency was set at 0.2 Hz. Photocurrent spectra (incident photon to current efficiency (IPCE) data) were plotted as a function of incident light wavelength (λ) ranging from 350 to 600 nm in steps of 5 nm. The light intensity was calibrated using a standard silicon photodiode. The light chopping frequency was set to 4.3+/−0.2 Hz to minimise attenuation affects. The apparatus consisted of a Stanford Research Systems SR830 (Stanford, USA) lock-in amplifier, a SR540 chopper controller, a home-built potentiostat, a 75 W xenon lamp powered by a Bentham 650 power supply, and a monochromator controller PMC3 B (Bentham Instruments Ltd, Reading, UK). The spectra were recorded using a home-built LabVIEW program. After annealing in vacuum electrochemical measurements of α-Fe$_2$O$_3$ films were started after 2 days equilibration in ambient conditions.

3. Results and discussion

The printed hematite films after annealing at 500 °C for 2 h in air have a bright orange color typical for hematite (Fig. 2) and are optically transparent. The XRD patterns for these films (Fig. 2) are consistent with the presence of only ITO substrate and hematite phase (α-Fe$_2$O$_3$ in hexagonal crystal system). The colour as well as the XRD pattern recorded for hematite films before and after vacuum annealing do not differ.

FE-SEM images for α-Fe$_2$O$_3$ films on the ITO substrate (both top view and cross-sectional) are shown in Fig. 3. The hematite material is formed with a nano-structure patterns of typically 20 nm feature size, and this is attributed here to the presence of the Brij® O10 surfactant in the ink phase. Similar types of pattern are produced/reported for example with block-co-polymers [40,41]. Cross-sectional images reveal a film thickness of typically 550 nm and grain sizes of 10–30 nm throughout the film.

Fig. 4A–D summarize the XPS results for two types of hematite films: (i) ambient annealed and (ii) vacuum annealed. Fig. 4A shows a survey spectrum with prominent signals for Fe and O. As seen in Fig. 4B, the peak positions of the Fe 2p signals do not differ substantially for both types of films. Satellite peaks at 715 eV and 729 eV
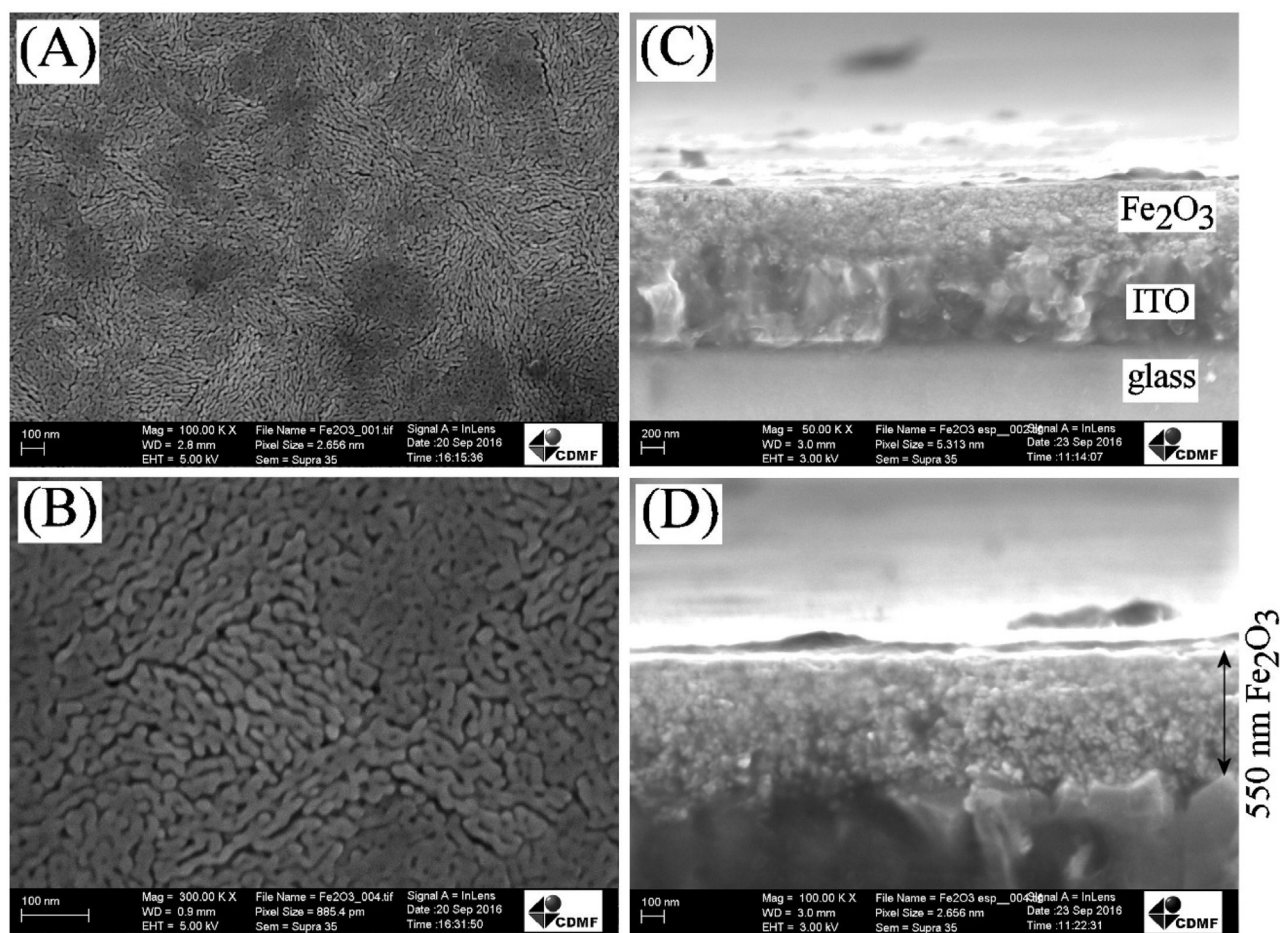
Fig. 3. FE-SEM images (top view (A,B) and cross-sectional (C,D)) of α-Fe$_2$O$_3$ film formed on ITO substrate.
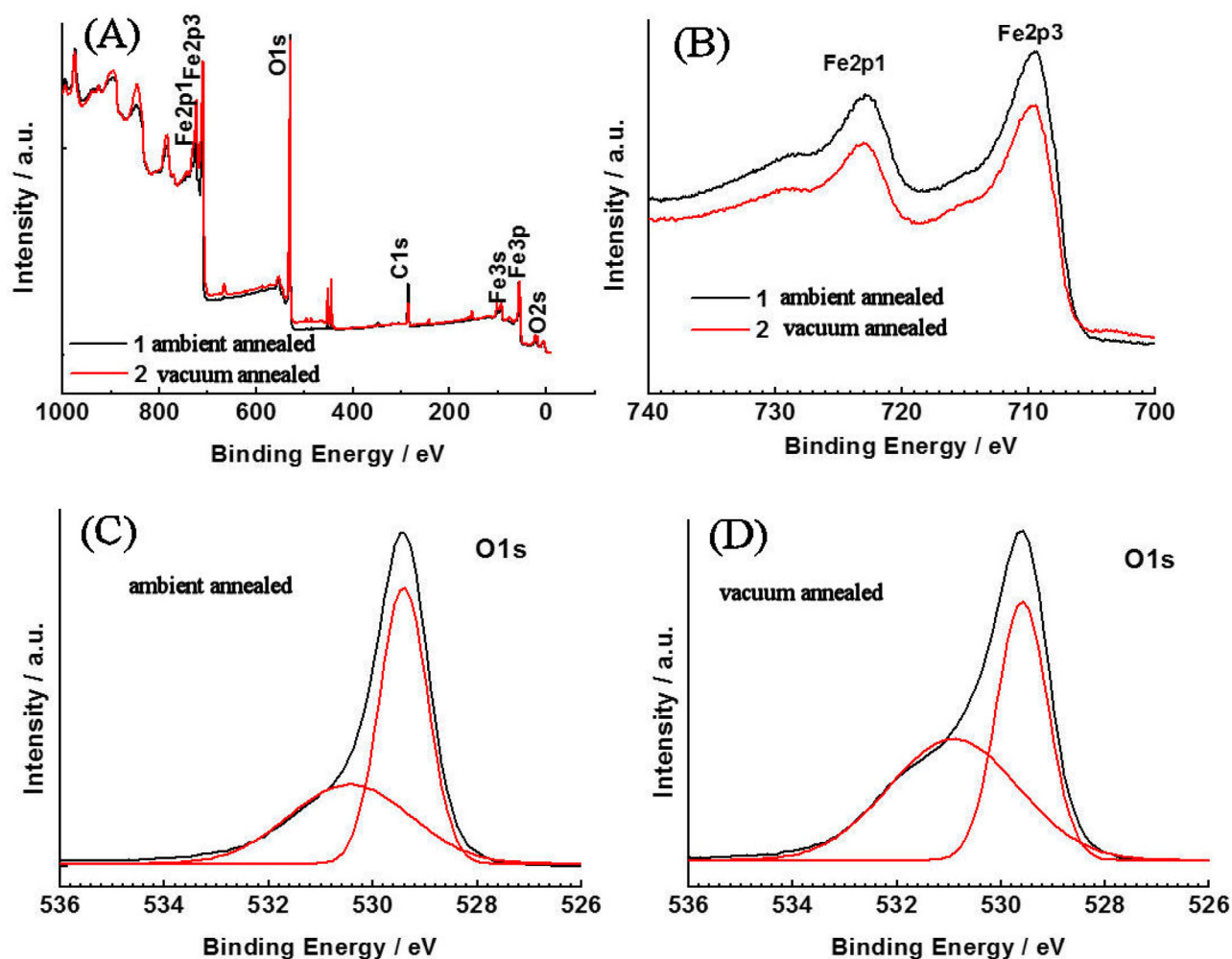
have in the past been attributed to presence of Fe(III) shake-up signals [37,42]. XPS signals for Fe(II) would be expected as shoulders, but are here not resolved probably due to low Fe(II) concentrations generated during vacuum-annealing. However, a more significant change is seen in the O 1 s peak shown in Fig. 4D. This peak can be deconvoluted into the main peak at 529.6 eV (oxygen atoms bound to Fe(III) at the surface) and a shoulder peak at 530.9 eV (attributed here to effects of surface hydration and possibly indicative of additional defect sites with hydroxide coordination [43]). For the hematite film which was ambient-annealed, the shoulder peak is less expressed in the O 1 s signal (Fig. 4C). In this case, the O 1 s peak can be deconvoluted into the main peak at 529.4 eV and the shoulder peak at 530.4 eV. The intensity for the shoulder peak is higher for the film, which was vacuum-annealed. This may suggest that annealing of hematite films *in vacuo* at 500 °C for 2 h followed by re-equilibration to room temperature leads to a significant increase in surface hydration, which may be linked to the number of near-surface oxygen vacancies. An improved hydration of the hematite surface may also be linked to a change in oxygen evolution reactivity, consistent with literature reports on reactive hydrated surface layers [44].

The photocurrent spectra (all obtained with back illumination) for typical α-Fe$_2$O$_3$ films recorded before and after annealing in vacuum at 500 °C are shown in Fig. 5. Spectral features with maximum at 387 nm are in good agreement with literature data [37] and reflect the ability of hematite to absorb photons of light followed by charge separation and photo-current response. The IPCE values are measured at anodic 0.1 V vs. SCE bias immersed in 0.1 M NaOH solution. The estimation of the band gap based on these spectra suggests
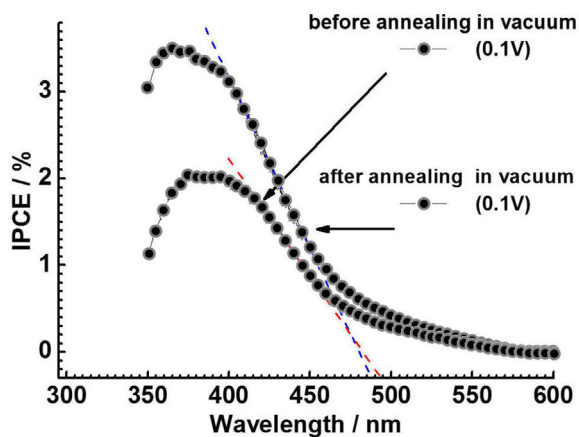
a value of approximately 2.4–2.5 eV (see lines in Fig. 5). This value is in good agreement with literature values of 1.9–2.5 eV [45–47]. Variation are usually attributed to grain size and crystallinity.

The effect of the vacuum annealing is clearly significant and therefore photo-transients are further investigated. The linear sweep voltammetry photo-transient data recorded before annealing of α-Fe$_2$O$_3$ film *in vacuo* and after are presented in Fig. 6. Before vacuum-annealing the typical photocurrent is limited at about 70 μA cm^{-2} at 0.4 V vs. SCE in 0.1 M NaOH electrolyte. This corresponds to a bias potential of approximately 1.4 V vs. RHE corresponding to relatively high bias (RHE = relative hydrogen electrode with $E_{RHE} = E_{SCE} + 0.98$ V). After vacuum-annealing of the α-Fe$_2$O$_3$ film, the photocurrent increased more than three-fold and reached 230 μA cm^{-2} at 0.4 V vs. SCE under the same conditions (Fig. 6).

It is interesting to explore some further features of the photo-transient data: (i) although the shape of photo-transient during light-on and light-off switching remains the same, the switching time constant $\tau = \frac{1}{k_{tr}+k_{rec}}$ appears to be faster after vacuum-annealing indicative possibly of an increase in k_{tr} and/or k_{rec}; (ii) the current response during light-off periods (see "hole accumulation" in Fig. 6A) is lower after vacuum-annealing indicative of less hole accumulation and an increase in k_{tr} and/or k_{rec}; (iii) although the photocurrents seem to saturate before vacuum-annealing, they appear to increase with applied potential after vacuum-annealing, indicative of a switch from a potential independent to potential dependent transport layer $\delta_{transport}$. These three observations are linked by the formation of the oxygen vacancies and sub surface

Fig. 4. Data for X-ray photoelectron spectroscopy (XPS) analysis. The survey spectra (A) and the Fe2p peaks (B) were recorded for the ambient-annealed (curve 1) and vacuum-annealed (curve 2) hematite films. The O 1 s peaks were obtained for (C) the film which was ambient-annealed and (D) the film after vacuum-annealing.
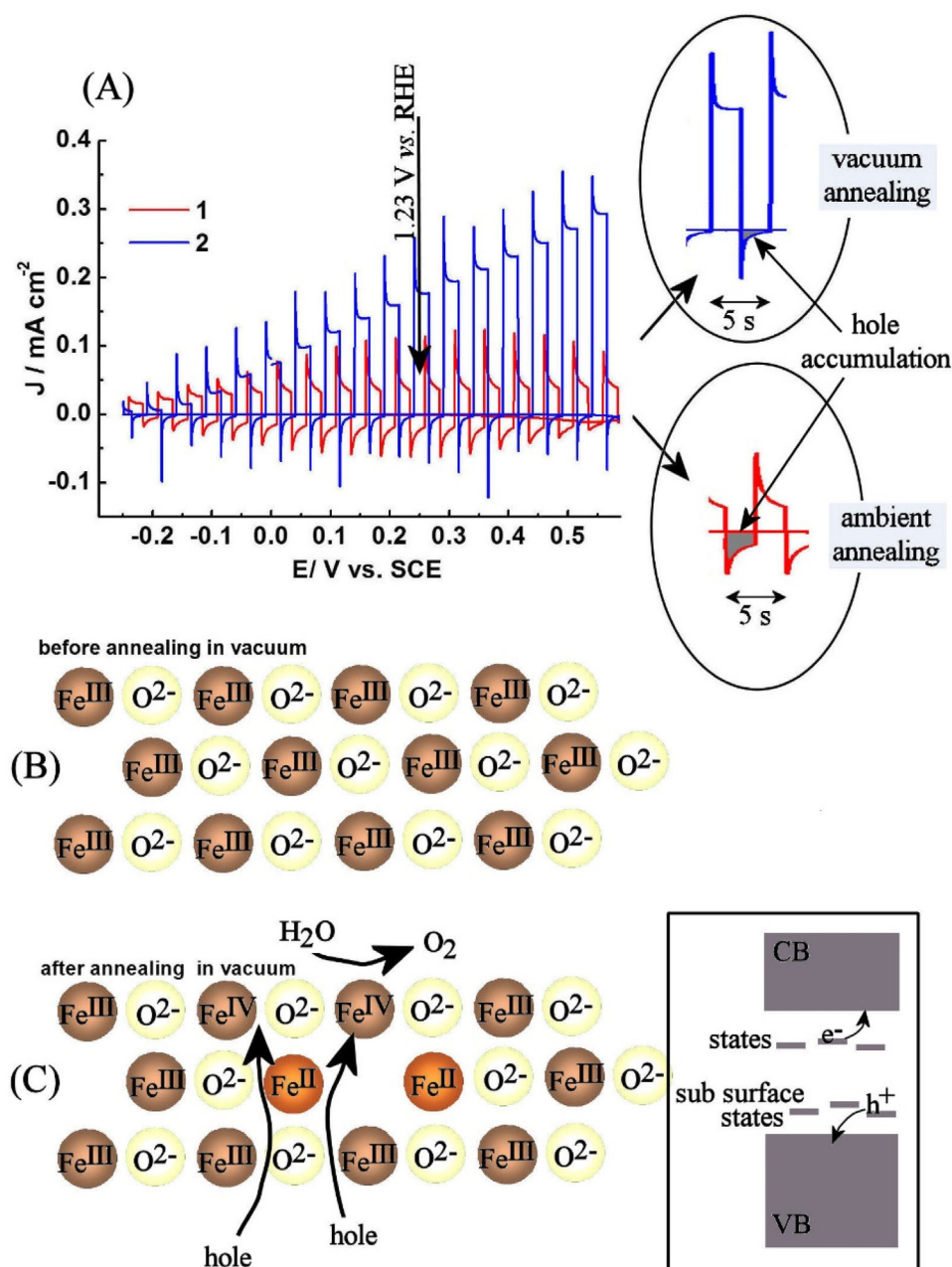

Fig. 5. The Incident Photon to Current Efficiency (IPCE) for a Fe_2O_3 film electrode in 0.1 M NaOH electrolyte at 0.1 V vs. SCE before and after vacuum-annealing at 500 °C for 2 h.

states and indicative mainly of a faster rate of transfer k_{tr}. It is interesting to compare to a similar effect induced by tin doping [48].

It is known that vacuum-annealing also causes an increase in electron conductivity in the underlying ITO film/contacts [49], which could be to some extent linked to the observed improvements in photo-electrochemical properties. However, when focusing on the hematite film, the enhancement of photo-electrochemical properties of α-Fe_2O_3 films is probably related to a loss of oxygen from surface, sub-surface, and from the crystal lattice during vacuum-annealing. Reports in the literature suggest formation of states below the conduction band to enhance electron mobility (see states in Fig. 6C). When charged positively and located close to the surface, these states may also allow transfer of holes to the surface (see "sub-surface states" in Fig. 6C). To date, several explanations of the role of oxygen vacancies in hematite have been proposed in the literature, such as blocking of slow surface hole-bulk electron recombination pathways by oxygen vacancies, increasing of carrier density as a result of the production of new oxygen vacancies in hematite, which leads to the enhanced oxygen evolution reaction activity, as well as higher charge separation yields and decreased contact resistances at the semiconductor/transparent conducting oxide interface [50]. All of these may be to some extent relevant. However, it is intriguing to also consider effects of sub-surface states [51] created when oxygen vacancies are generated under vacuum annealing conditions (see Fig. 6C). The presence of these states in the bulk is consistent with *n*-doping and therefore related to enhanced electron transport. But the sub-surface states may also allow holes to reach lower-lying surface states, which could have the effect of a "conduit" allowing holes to emerge at high concentration at a specific

Fig. 6. (A) Cyclic voltammetry (scan rate 10 mV s^{-1}) for a Fe$_2$O$_3$ film electrode immersed in 0.1 M NaOH electrolyte under pulsed blue light (λ = 455 nm, 0.2 Hz) before (curve 1) and after (curve 2) vacuum-annealing at 500 °C for 2 h. (B,C) Schematic drawing of the hematite lattice before and after vacuum annealing highlighting the role of sub surface states in the catalytic process.

surface site, which will cause a higher reactivity towards oxygen evolution (*i.e.* an increase in k_{tr}). Furthermore, the formation of an oxygen molecule (which is released into the vacuum under thermal annealing conditions) will provide exactly four Fe(II) sites in close vicinity and these four sites may then work in a concerted manner in the ambient photo-electrochemical oxygen evolution process to give a higher k_{tr}. The hypothesis of a possible mechanistic link of thermal oxygen release into vacuum and photo-electrochemical oxygen production and the role of sub-surface states will require further investigation.

4. Conclusion

Transparent films of α-Fe$_2$O$_3$ were prepared on ITO substrates by inkjet printing with subsequent annealing at 500 °C for 2 h in air.

XRD analysis confirmed the presence of hematite phase (α-Fe$_2$O$_3$, hexagonal crystal system) without other iron oxides or impurities. It was found that thermal vacuum-annealing at 500 °C for 2 h substantially improves the photocurrents, which increased more than three times, from 70 μA cm^{-2} to 230 μA cm^{-2} (under LED illumination, λ = 455 nm, ca. 100 mW cm^{-2}) at 0.4 V vs. SCE in 0.1 M NaOH electrolyte. The enhancement of photocurrent is accompanied by the increase of incident photon to current efficiency. The improvement of photoelectrical properties observed for ink-jet printed hematite films is attributed here to the loss of oxygen/formation of oxygen vacancies during vacuum-annealing. Indirect evidence of oxygen vacancies after vacuum-annealing has been obtained by the XPS analysis and a link between oxygen vacancies and surface reactivity appears plausible. However, the mechanism by which the photo-currents are increased is currently not fully understood.

This study is preliminary in nature and more detailed data will be needed (e.g. controlling the vacuum-annealing conditions to explore effects from the number and depth of vacancies) to shed further light onto the mechanisms responsible for photocurrent enhancement and to allow optimization of conditions for device production. Ink-jetting as a methodology for the preparation of hematite films is attractive, although the photo-electrochemical performance of films reported here appears limited even after vacuum annealing. Further improvements in the ink-jetting recipe (e.g. different surfactants, other types of ligands on the Fe(III) precursor, more control during deposition, additional ligand control over the thermal mineralization process, etc.) will be needed to further improve the hematite micro-structure.

Acknowledgements

References

[1] F. Yilmaz, M.T. Balta, R. Selbas, Renew. Sustain. Energy Rev. 56 (2016) 171–178.
[2] R. van de Krol, Y. Liang, J. Schoonman, J. Mater. Chem. 18 (2008) 2311–2320.
[3] L.M. Peter, K.G.U. Wijayantha, ChemPhysChem 15 (2014) 1983–1995.
[4] S. Shen, S.A. Lindley, X. Chen, J.Z. Zhang, Energy Environ. Sci. 9 (2016) 2744–2775.
[5] F.E. Osterloh, Chem. Soc. Rev. 42 (2013) 2294–2320.
[6] D.A. Wheeler, G.M. Wang, Y.C. Ling, Y. Li, J.Z. Zhang, Energy Environm. Sci. 5 (2012) 6682–6702.
[7] L.M. Peter, J. Solid State Electrochem. 17 (2013) 315–326.
[8] M. Barroso, C.A. Mesa, S.R. Pendlebury, A.J. Cowan, T. Hisatomi, K. Sivula, M. Grätzel, D.R. Klug, J.R. Durrant, PNAS 109 (2012) 15640–15645.
[9] K. Sivula, F. Le Formal, M. Grätzel, ChemSusChem 4 (2011) 432–449.
[10] J.A. Glasscock, P.R.F. Barnes, I.C. Plumb, A. Bendavid, P.J. Martin, Thin Solid Films 516 (2008) 1716–1724.
[11] T.W. Hamann, Dalton Trans. 41 (2012) 7830–7834.
[12] K.X. Wang, Z. Yu, V. Liu, M.L. Brongersma, T.F. Jaramillo, S. Fan, ACS Photonics 1 (2014) 235–240.
[13] K.G.U. Wijayantha, S. Saremi-Yarahmadi, L.M. Peter, Phys. Chem. Chem. Phys. 13 (2011) 5264–5270.
[14] C.Y. Cummings, F. Marken, L.M. Peter, K.G.U. Wijayantha, A.A. Tahir, J. Am. Chem. Soc. 134 (2012) 1228–1234.
[15] A.G. Tamieat, J. Rick, A.A. Dubale, W.N. Su, B.J. Hwang, Nanosc. Horiz. 1 (2016) 243–267.
[16] J.H. Kennedy, K.W. Frese, J. Electrochem. Soc. 125 (1978) 709–714.
[17] F. Le Formal, K. Sivula, M. Grätzel, J. Phys. Chem. C 116 (2012) 26707–26720.
[18] D. Benjelloun, J.P. Bonnet, J.P. Doumerc, J.C. Launay, M. Onillon, P. Hagenmuller, Mater. Chem. Phys. 10 (1984) 503–510.
[19] K.M. Rosso, D.M.A. Smith, M. Dupuis, J. Chem. Phys. 118 (2003) 6455–6466.
[20] N. Iordanova, M. Dupuis, K.M. Rosso, J. Chem. Phys. 122 (2005) 144305–144310.
[21] L.A. Marusak, R. Messier, W.B. White, J. Phys. Chem. Solids 41 (1980) 981–984.
[22] Z. Li, W. Luo, M. Zhang, J. Feng, Z. Zou, Energy Environ. Sci. 6 (2013) 347–370.
[23] M.N. Huda, A. Walsh, Y.F. Yan, S.H. Wei, M.M. Al-Jassim, J. Appl. Phys. 107 (2010) 123712.
[24] F. Boudoire, R. Toth, J. Heier, A. Braun, E.C. Constable, Energy Environ. Sci. 7 (2014) 2680–2688.
[25] J. Yang, C.X. Bao, T. Yu, Y.F. Hu, W.J. Luo, W.D. Zhu, G. Fu, Z.S. Li, H. Gao, F.M. Li, Z.G. Zou, ACS Appl. Mater. Interf. 7 (2015) 26482–26490.
[26] H. Gao, C. Liu, H.E. Jeong, P. Yang, ACS Nano 6 (2012) 234–240.
[27] A.G. Tamirat, W.N. Su, A.A. Dubale, C.J. Pan, H.M. Chen, D.W. Ayele, J.F. Lee, B.J. Hwang, J. Power Sourc. 287 (2015) 119–128.
[28] T. Hisatomi, F. Le Formal, M. Cornuz, J. Brillet, N. Tetreault, K. Sivula, M. Grätzel, Energy Environ. Sci. 4 (2011) 2512–2515.
[29] M.G. Ahmed, I.E. Kretschmer, T.A. Kandiel, A.Y. Ahmed, F.A. Rashwan, D.W. Bahnemann, ACS Appl. Mater. Interf. 7 (2015) 24053–24062.
[30] S.D. Tilley, M. Cornuz, K. Sivula, M. Grätzel, Angew. Chem. Int. Ed. 49 (2010) 6405–6552.
[31] K.J. McDonald, K.S. Choi, Chem. Mater. 23 (2011) 4863–4869.
[32] J.W. Moir, E.V. Sackville, U. Hintermair, G.A. Ozin, J. Phys. Chem. C 120 (2016) 12999–13012.
[33] M. Forster, R.J. Potter, Y. Ling, Y. Yang, D.R. Klug, Y. Li, A.J. Cowan, Chem. Sci. 6 (2015) 4009–4016.
[34] J. Moir, N. Soheilnia, K. Liao, P. O'Brien, Y. Tian, K.S. Burch, G.A. Ozin, ChemSusChem 8 (2015) 1557–1567.
[35] C. Zhu, C. Li, M. Zheng, J.J. Delaunay, ACS Appl. Mater. Interf. 7 (2015) 22355–22363.
[36] T.Y. Yang, H.Y. Kang, U. Sim, Y.J. Lee, J.H. Lee, B. Koo, K.T. Nam, Y.C. Joo, Phys. Chem. Chem. Phys. 15 (2013) 2117–2124.
[37] Y.C. Ling, G.M. Wang, J. Reddy, C.C. Wang, J.Z. Zhang, Y. Li, Angew. Chem. Internat. Ed. 51 (2012) 4074–4079.
[38] C.Y. Cummings, F. Marken, L.M. Peter, A.A. Tahir, K.G.U. Wijayantha, Chem. Commun. 48 (2012) 2027–2029.
[39] L.M. Peter, J. Li, R. Peat, J. Electroanal. Chem. 165 (1984) 29–40.
[40] K. Brezesinski, J. Haetge, J. Wang, S. Mascotto, C. Reitz, A. Rein, S.H. Tolbert, J. Perlich, B. Dunn, T. Brezesinski, Small 7 (2011) 407–414.
[41] C. Henrist, C. Toussaint, J. de Vroede, D. Chatzikyriakou, J. Dewalque, P. Colson, A. Maho, R. Cloots, Micropor. Mesopor. Mater. 221 (2016) 182–186.
[42] T. Fujii, F.M.F. de Groot, G.A. Sawatzky, F.C. Voogt, T. Hibma, K. Okada, Phys. Rev. B 59 (1999) 3195–3202.
[43] G.S. Parkinson, Surf. Sci. Rep. 71 (2016) 272–365.
[44] M.E.G. Lyons, R.L. Doyle, D. Fernandez, I.J. Godwin, M.P. Browne, A. Rovetta, Electrochem. Commun. 45 (2014) 56–59.
[45] B. Gilbert, C. Frandsen, E.R. Maxey, D.M. Sherman, Phys. Rev. B 79 (2009) 035108–035114.
[46] R.N. Goyal, A.K. Pandey, D. Kaur, A. Kumar, J. Nanosci. Nanotechnol. (2009) 4692–4701.
[47] D.H. Taffa, I. Hamm, C. Dunkel, I. Sinev, D. Bahnemanncd, M. Wark, RSC Adv. 5 (2015) 103512–103517.
[48] H.K. Dunn, J.M. Feckl, A. Müller, D. Fattakhova-Rohlfing, S.G. Morehead, J. Roos, L.M. Peter, C. Scheu, T. Bein, Phys. Chem. Chem. Phys. 16 (2014) 24610–24620.
[49] A.M. Collins, G.J. Blanchard, F. Marken, Electroanalysis 24 (2012) 246–253.
[50] M. Barroso, S.R. Pendlebury, A.J. Cowan, J.R. Durrant, Chem. Sci. 4 (2013) 2724–2730.
[51] D.K. Bora, Y.L. Hu, S. Thiess, S. Erat, X.F. Feng, S. Mukherjee, G. Fortunato, N. Gaillard, R. Toth, K. Gajda-Schrantz, W. Drube, M. Grätzel, J.H. Guo, J.F. Zhu, E.C. Constable, D.D. Sarma, H.X. Wang, A. Braun, J. Electron Spectr. Rel. Phenom. 190 (2013) 93–105.